Full quantum simulation of Shockley–Read–Hall recombination in p-i-n and tunnel diodes☆

A. Pilotto *, P. Dollfus, J. Saint-Martin, M. Pala

Université Paris-Saclay, CNRS, C2N, 10 Boulevard Thomas Gobert, 91120 Palaiseau, France

ARTICLE INFO

ABSTRACT

We have included Shockley–Read–Hall (SRH) generation/recombination in Non-equilibrium Green's function (NEGF) calculations via a multiphonon relaxation model. The model has been used to study how the presence of defects affects the current–voltage characteristics of GaAs p-i-n diodes, and of an InGaAs tunnel diode. Regarding p-i-n diodes, we show that SRH generation/recombination is responsible for ideality factors approaching the theoretical value of two in the forward bias regime, while in reverse bias the recombination current density varies slowly with the applied voltage. In all the considered cases, the defects located in the center of the active region proved to be the most effective in allowing trap-assisted tunneling from the valence to the conduction band. Finally, the inclusion of SRH recombination in NEGF simulations of Esaki tunnel diodes permits to predict a realistic degradation of the peak-to-valley current ratio.

1. Introduction

Trap assisted generation/recombination of electron and holes occurring in the active region of electron devices is known to be a limiting factor of their electrical performance. For instance, the *dark count rate* of single photon avalanche diodes (SPADs) is largely influenced by impact ionization of thermally generated carriers that, at large electric fields, trigger undesired avalanche multiplication and induce false photon detection [1,2]. At the same time, empty traps can be filled during the avalanche subsequent to the generation of electron–hole pairs induced by photon absorption. Detrapping of these charged states at a later time is the cause of secondary pulses in the current waveform (*after pulsing*) that are erroneously interpreted as photon counts [1,3]. On the other hand, in Esaki diodes, recombination induced by defect states is one of the main contributors to the degradation of the *peak-to-valley current ratio* in the forward bias regime [4,5].

An accurate modeling of defect-mediated generation/recombination is therefore of fundamental importance for the correct assessment of the behavior of semiconductor diodes and, in the literature, many models to treat this problem can be found, ranging from semiclassical [7] to full-quantum approaches [8–10]. Recently, a model to include Shockey–Read–Hall (SRH) type recombination [6,11] via nonradiative multiphonon relaxation [12] in NEGF calculations has been proposed in [13], and successfully applied to study forward biased p-i-n junctions [13] and LEDs [14]. In this paper, we use the model of [13] to study the impact of SRH recombination occurring at different device
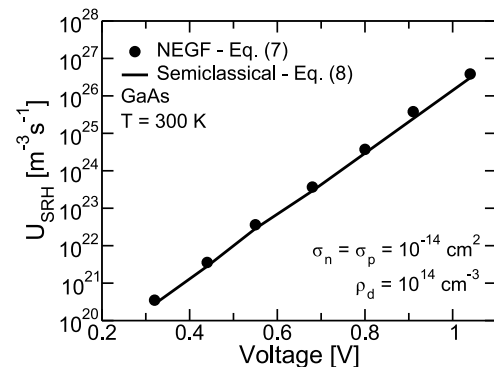
Fig. 1. Recombination rate in bulk GaAs as a function of the applied bias voltage. Results obtained by using the NEGF formalism (Eq. (7), symbols) are compared to the semiclassical expression [6] (Eq. (8), lines) for $\sigma_n = \sigma_p = 10^{-14}$ cm^2 and $\rho_d = 10^{14}$ cm^{-3}.

regions on the *forward and reverse* current–voltage characteristics ($I - V$) of GaAs p-i-n junctions and of an InGaAs Esaki diode. The paper proceeds as follows: Section 2 briefly describes the model of [13] and its implementation. Results obtained by simulations of bulk GaAs, GaAs p-i-n diodes, and of an InGaAs Esaki diode are shown in Section 3. Finally, Section 4 reports our concluding remarks.
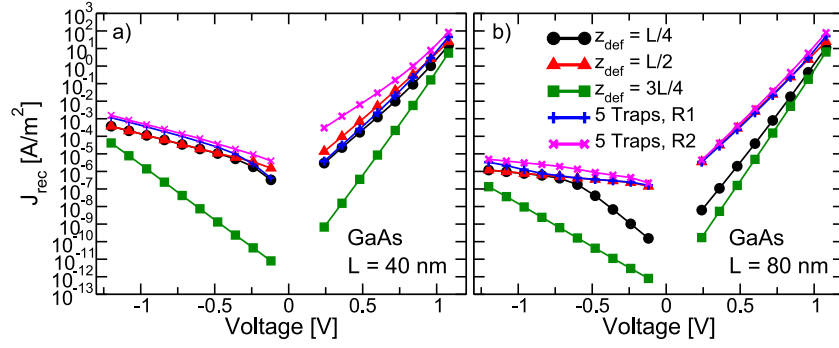
Fig. 2. Recombination current as a function of the applied voltage for GaAs p-i-n diodes with intrinsic regions thickness (a) $L = 40$ nm and (b) 80 nm. Different configurations have been considered: single midgap defects located at $L/4$ (black circles), $L/2$ (red triangles), $3L/4$ (green squares) and two random distributions of five traps (blue plus signs and magenta crosses). $\sigma_n = \sigma_p = 5 \times 10^{-14}$ cm^2 and $\rho_d = 10^{13}$ cm^{-3}.
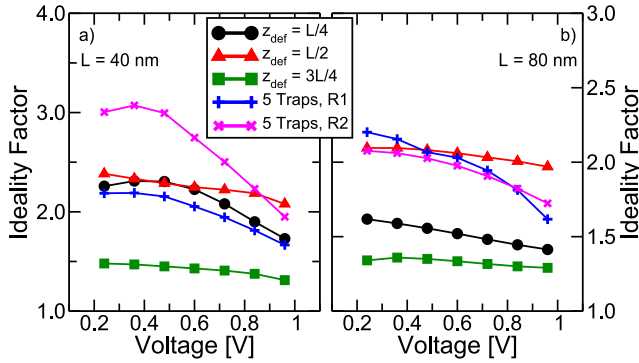
Fig. 3. Ideality factors in forward bias for the p-i-n diodes and the trap configurations of Fig. 2.

2. Model description

The model for the treatment of SRH recombination via multiphonon relaxation in NEGF calculations [13] assumes that the defect density is strongly localized in space and energy, and, in the case of a structure with confinement along the z direction, it is therefore represented by a Dirac's delta function at $z = z_{def}$ and $E = E_{def}$.

Here, as in [13,14], the Dyson's equation for the retarded Green's function of the defect (G_d) is not solved, but, instead, the lesser-than and greater-than Green's functions ($G_d^<$ and $G_d^>$, respectively) are computed by using the quasi-equilibrium expressions

$$G_d^<(E) = i f_d(E) A_d(E),$$ (1)

$$G_d^>(E) = -i(1 - f_d(E)) A_d(E),$$ (2)

where A_d is the defect's spectral function and f_d describes the defect's occupation. The value of $f_d(E = E_{def})$ can be derived from the balance at steady-state between the capture and emission rates [13], namely

$$f_d(E_{def}) = -i \frac{\Sigma_{dc}^<(E_{def}) + \Sigma_{dv}^<(E_{def})}{\Gamma_{dc}(E_{def}) + \Gamma_{dv}(E_{def})},$$ (3)

where $\Gamma = i(\Sigma^> - \Sigma^<)$.

In the case of electrons, the self-energies that describe carrier capture/emission into/from the defect state and into/from the bands are computed with Eqs. (4) and (5), respectively.

$$\Sigma_{dc}^{\lessgtr}(z_{def}, E) = \frac{1}{A} \sum_{\mathbf{k}_\parallel} \sum_{l \geq 0} \mathcal{M}_{em/capt}(l)$$
$$\times \int dz G_c^{\lessgtr}(\mathbf{k}_\parallel, z, z, E + l\hbar\Omega_0) \delta(z - z_{def})$$ (4)

$$\Sigma_{cd}^{\lessgtr}(z, z, E) = \rho_d \sum_{l \geq 0} \mathcal{M}_{em/capt}(l) G_d^{\lessgtr}(E - l\hbar\Omega_0) \delta(z - z_{def})$$ (5)

Table 1
Parameters used throughout this paper.

Material	m_e [m_0]	m_h [m_0]	E_g [eV]	S	$\hbar\Omega_0$ [meV]
GaAs	0.067	0.51	1.42	3.5 [12]	36
InGaAs	0.041	0.45	0.74	0.4 [15]	34

$$\mathcal{M}_{capt}(l) = \mathcal{M}_{dc}^0 \frac{(l - S)^2}{S} e^{-S(2f_{BE}+1)} \left(\frac{f_{BE} + 1}{f_{BE}} \right)^{l/2} \mathcal{I}_l \left(2S \sqrt{f_{BE}(f_{BE} + 1)} \right)$$ (6)

where ρ_d is the defect density, Ω_0 is the phonon frequency, l identifies the number of phonons involved in the recombination process, S is the Huang–Rhys factor, f_{BE} is the phonon occupation given by the Bose–Einstein distribution, $\mathcal{I}_l$ is the modified Bessel function of lth order, and $\mathcal{M}_{em}(l) = \mathcal{M}_{capt} e^{-l\hbar\Omega_0/k_B T}$. Expressions similar to Eqs. (4), (5) are used to compute the self-energies (Σ_{dc} and Σ_{vd}) for the coupling between the defect and valence band states. The constants $\mathcal{M}_{dc}^0$ and $\mathcal{M}_{dv}^0$ are linked to the carrier thermal velocities ($v_{th,n/p}$) and capture cross sections ($\sigma_{n/p}$) as described in [13].

Finally, current conservation is obtained by self-consistently solving the equations for the retarded and the lesser(greater)-than Green's functions.

3. Results

This section reports the results of the simulations of bulk GaAs, GaAs p-i-n diodes and an InGaAs p-i-n diode when the method reported in Section 2 is used. In the following, the parameters reported in Table 1 have been employed. Defect states have always assumed to be located at midgap.

3.1. Bulk GaAs

As a validation of our implementation, we have verified that the recombination rate computed by using the aforementioned approach (Eq. (7)) is equivalent to the semiclassical expression (Eq. (8)) [6] when the carrier lifetimes are $\tau_{n/p} = \rho_d \sigma_{n/p} v_{th,n/p}$ and the electron and hole densities are obtained from NEGF calculations. The results in Fig. 1, obtained by using an effective mass Hamiltonian with two parabolic bands (see Table 1), and for a defect density $\rho_d = 10^{14}$ cm^{-3} show an excellent agreement between Eqs. (7) and (8).

$$U_{SRH} = \rho_d \int \frac{dE}{2\pi\hbar} \left[\Sigma_{dc}^<(E) G_d^>(E) - \Sigma_{dc}^>(E) G_d^<(E) \right]$$ (7)

$$U_{SRH} = \frac{np - n_{eq} p_{eq}}{\tau_p(n + n_1) + \tau_n(p + p_1)}$$ (8)
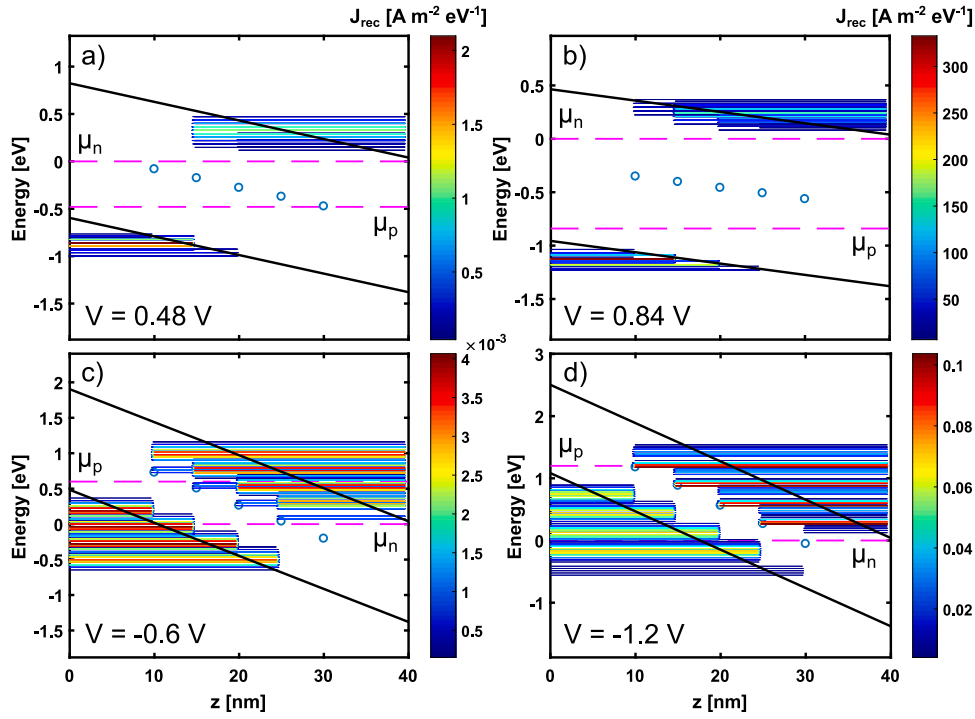
Fig. 4. Spectral recombination current density at (a) $V = 0.48$ V, (b) $V = 0.84$ V, (c) $V = -0.6$ V, and (d) $V = -1.2$ V of a 40 nm long GaAs p-i-n diode when five midgap defects from $z = 10$ nm to $z = 30$ nm are simulated (blue circles). $\sigma_n = \sigma_p = 5 \times 10^{-14}$ cm^2 and $\rho_d = 10^{13}$ cm^{-3}.

3.2. GaAs p-i-n diodes

We have employed the model to simulate the recombination current characteristics of GaAs p-i-n diodes with different thickness of the intrinsic region ($L = 40$ nm and $L = 80$ nm). A doping concentration $N_d = N_a = 10^{17}$ cm^{-3} has been assumed in both contact regions and a linear potential profile across the intrinsic layer has been considered. For the two diodes, five different traps configurations have been analyzed: a single midgap defect located at $z_{def} = L/4$, $L/2$, or $3L/4$ and two random distributions of five traps, namely $R1_{40} = [4 \text{ nm}, 7.6 \text{ nm}, 10 \text{ nm}, 23.3 \text{ nm}, 39.2 \text{ nm}]$, $R2_{40} = [10 \text{ nm}, 15 \text{ nm}, 20 \text{ nm}, 25 \text{ nm}, 30 \text{ nm}]$ for the 40 nm diode, and $R1_{80} = [10 \text{ nm}, 11.6 \text{ nm}, 15.2 \text{ nm}, 32.8 \text{ nm}, 57.2 \text{ nm}]$, $R2_{80} = [20 \text{ nm}, 30 \text{ nm}, 40 \text{ nm}, 50 \text{ nm}, 60 \text{ nm}]$ for the thicker diode. Recombination currents are shown in Fig. 2. As expected, in forward bias the recombination current increases with ideality factors that approach or exceed two (see Fig. 3). Ideality factors larger than two arise from the enhancement of the trap-assisted tunneling process provided by the band bending; this phenomenon is particularly relevant for thin diodes. On the other hand, in reverse bias configurations the recombination current is slowly varying with the applied bias, except for those cases where a single defect is located far from the center of the intrinsic region. In fact, by looking at the spectral current densities in Fig. 4, we notice that, due to the position of the defect with respect to the Fermi levels of the contacts, tunneling mediated by traps located at the center of the intrinsic region is the one that mostly affects the recombination current, while recombination at other locations becomes significant only for large applied bias voltages.

3.3. InGaAs Esaki diode

Finally, we have simulated a typical InGaAs Esaki diode composed of two degenerate contact regions ($N_a = 3 \times 10^{19}$ cm^{-3}, $N_d = 10^{19}$ cm^{-3}) separated by a 3 nm thick undoped layer. A two-bands **k·p** Hamiltonian has been used to simulate the coupling between the VB and the CB [16]. The coupling term has been treated as an adjustable parameter and it
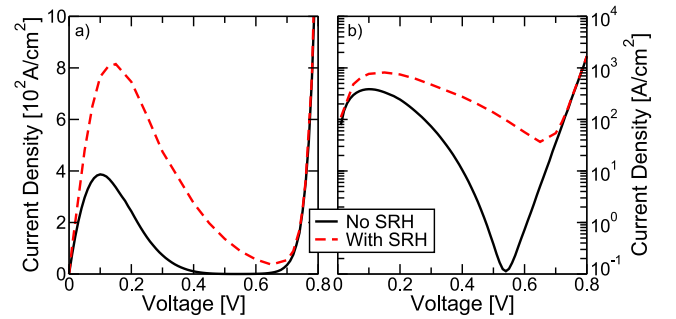
Fig. 5. $I - V$ characteristics in (a) linear and (b) log scales of an InGaAs Esaki diode when SRH recombination is neglected (solid black line) or included (dashed red line). $\sigma_n = \sigma_p = 10^{-15}$ cm^2 and $\rho_d = 2 \times 10^{11}$ cm^{-3}.

has been chosen in order to yield the correct curvature of the bands at the minimum/maximum. The potential profile has been derived from the self-consistent solution of the Poisson-NEGF equations. Fig. 6 compares the diode's $I - V$ characteristics with and without the SRH recombination. We notice that the inclusion of recombination in the simulations translates into a higher current peak, a larger lobe of the $I - V$ curve and also into a larger valley current. The effect of SRH recombination is illustrated by Fig. 6: while at $V = 0.1$ V (i.e. close to the peak-current voltage) both the recombination and the tunneling component contribute to the current density, only the former one determines the valley current.

4. Conclusions

We have employed a quantum model to include SRH recombination in NEGF simulations. The model has been used to study how the defect location in the active region of p-i-n diodes affects the characteristics of these devices, showing that SRH generation/recombination via multiphonon relaxation mostly occurs at defects located close to the center
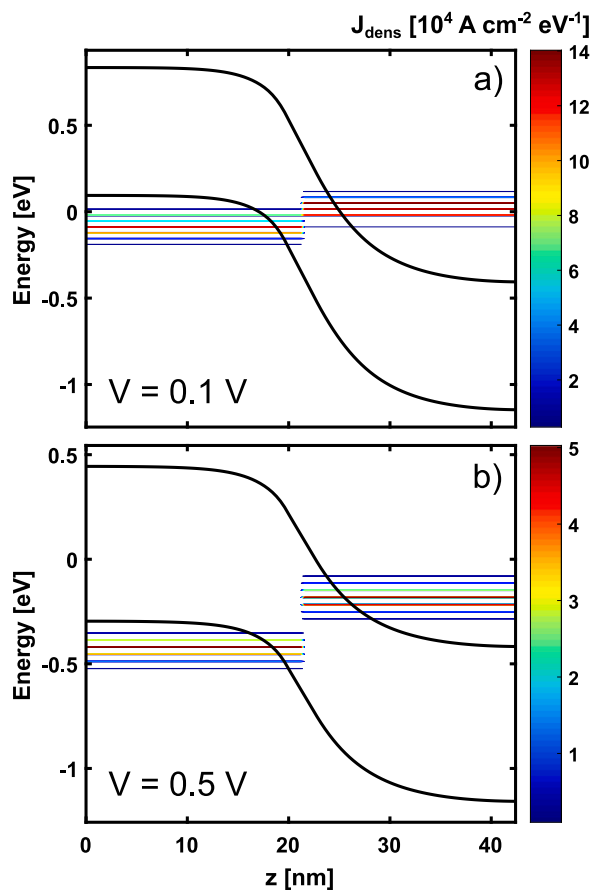
Fig. 6. Spectral current density at (a) $V = 0.1$ V and (b) $V = 0.5$ V for the InGaAs Esaki diode of Fig. 5.

of the diode's active region, due to the relative position of these trap states with respect to the Fermi levels of the contacts. In the simulation of Esaki tunnel diodes, the inclusion of the SRH recombination is able to predict the increase of the valley currents and the corresponding degradation of the peak-to-valley current ratio (from 3400 to 22). Therefore, this model can shed light on the role played by traps in the current characteristics of low-power devices such as the tunnel-FET.

Declaration of competing interest

The authors declare that they have no known competing financial interests or personal relationships that could have appeared to influence the work reported in this paper.

References

[1] Bronzi D, Villa F, Tisa S, Tosi A, Zappa F. SPAD figures of merit for photon-counting, photon-timing, and imaging applications: A review. IEEE Sens J 2016;16(1):3–12. http://dx.doi.org/10.1109/JSEN.2015.2483565.

[2] Panglosse A, Martin-Gonthier P, Marcelot O, Virmontois C, Saint-Pé O, Magnan P. Dark count rate modeling in single-photon avalanche diodes. IEEE Trans Circuits Syst I Regul Pap 2020;67(5):1507–15. http://dx.doi.org/10.1109/TCSI.2020.2971108.

[3] Vilà A, Arbat A, Vilella E, Dieguez A. Geiger-mode avalanche photodiodes in standard CMOS technologies. In: Gateva S, editor. Photodetectors. Rijeka: IntechOpen; 2012, ch. 9.

[4] Meyerhofer D, Brown GA, Sommers HS. Degenerate Germanium. I. Tunnel, excess, and thermal current in tunnel diodes. Phys Rev 1962;126:1329–41. http://dx.doi.org/10.1103/PhysRev.126.1329.

[5] Schenk A, Sant S. Tunneling between density-of-state tails: Theory and effect on Esaki diodes. J Appl Phys 2020;128(1):014502. http://dx.doi.org/10.1063/5.0008709.

[6] Shockley W, Read WT. Statistics of the recombinations of holes and electrons. Phys Rev 1952;87:835–42. http://dx.doi.org/10.1103/PhysRev.87.835.

[7] Sentaurus device user guide, version L-2016.03. Mountain View, CA, USA: Synopsys; 2016.

[8] Pala MG, Esseni D. Interface traps in InAs nanowire tunnel-FETs and MOSFETs-Part I: Model description and single trap analysis in tunnel-FETs. IEEE Trans Electron Devices 2013;60(9):2795–801. http://dx.doi.org/10.1109/TED.2013.2274196.

[9] Shao Y, Pala MG, Esseni D, del Alamo JA. Sub-10-nm diameter GaSb/InAs vertical nanowire Esaki diodes with ideal scaling behavior: Experiments and simulations. In: 2021 IEEE international electron devices meeting. IEDM, 2021, p. 32.1.1–4. http://dx.doi.org/10.1109/IEDM19574.2021.9720540.

[10] Shao Y, Pala M, Esseni D, del Alamo JA. Scaling of GaSb/InAs vertical nanowire Esaki diodes down to sub-10-nm diameter. IEEE Trans Electron Devices 2022;69(4):2188–95. http://dx.doi.org/10.1109/TED.2022.3145767.

[11] Hall RN. Electron-hole recombination in Germanium. Phys Rev 1952;87:387. http://dx.doi.org/10.1103/PhysRev.87.387.

[12] Schenk A. An improved approach to the Shockley–Read–Hall recombination in inhomogeneous fields of space-charge regions. J Appl Phys 1992;71(7):3339–49. http://dx.doi.org/10.1063/1.350929.

[13] Aeberhard U. Nonequilibrium Green's function picture of nonradiative recombination of the Shockley-Read-Hall type. Phys Rev B 2019;99:125302. http://dx.doi.org/10.1103/PhysRevB.99.125302.

[14] Gonzalez Montoya JA, Tibaldi A, De Santi C, Meneghini M, Goano M, Bertazzi F. Nonequilibrium Green's function modeling of trap-assisted tunneling in In$_x$Ga$_{1-x}$N/GaN light-emitting diodes. Phys Rev Appl 2021;16:044023. http://dx.doi.org/10.1103/PhysRevApplied.16.044023.

[15] Schenk A, Sant S, Moselund K, Riel H. Comparative simulation study of InAs/Si and all-III-V hetero tunnel FETs. ECS Trans 2015;66(5):157–69. http://dx.doi.org/10.1149/06605.0157ecst.

[16] Kane E. Zener tunneling in semiconductors. J Phys Chem Solids 1960;12(2):181–8. http://dx.doi.org/10.1016/0022-3697(60)90035-4.